Supporting Information

A Spiroacridine-Based Thermally Activated Delayed Fluorescence Emitter for High-Efficiency and Narrow-Band Deep-Blue OLEDs

Yong Huang, [‡a] Mengjiao Jia, [‡a] Chuan Li, [a] Yang Yang, [a] Yuling He, [a] Yanju Luo, [*b]
Yan Huang, [a] Liang Zhou, [*c] and Zhiyun Lu [*a]

[a] *Key Laboratory of Green Chemistry and Technology (Ministry of Education), College of Chemistry, Sichuan University, Chengdu, Sichuan 610064, China. E-mail: luzhiyun@scu.edu.cn.*

[b] *Analytical & Testing Center, Sichuan University, Chengdu, Sichuan 610064, China. E-mail: luoyanju@scu.edu.cn.*

[c] *State Key Laboratory of Rare Earth Resource Utilization Changchun Institute of Applied Chemistry Chinese Academy of Sciences, Changchun, 130022, China. E-mail: zhoul@ciac.ac.cn.*

I. Experimental details

1. General Information

Materials. Unless otherwise described, all reagents and anhydrous solvents were purchased from commercial sources and used without further purification. All the solvents used in photophysical measurements were of analytical grades and freshly distilled before use. The target compound **SAC-BOC** was purified through three times recrystallization followed by vacuum sublimation. **DPEPO** and other OLED materials were purchased from Luminescence Technology Corporation and were used without further purification.

General method. ^{1}H NMR and ^{13}C NMR spectra were recorded on a Bruker AVANCE II-400 MHz spectrometer at 400 and 100 MHz in CDCl$_3$, respectively. Tetramethylsilane (TMS) was used as an internal standard. All chemical shift data were reported in the standard δ notation of parts per million (ppm). Splitting patterns were designed as follows: s (singlet), d (doublet), t (triplet) and m (multiplet). High resolution MS spectra were measured on a Q-TOF Premier ESI mass spectrometer (Micromass, Manchester, UK). UV-visible absorption spectra were measured on an AOE A590 spectrophotometer. Steady-state photoluminescence (PL) spectra at room temperature (RT) and phosphorescence spectra at 77 K were measured on a Horiba Jobin Yvon Fluoromax-Plus-P fluorescence spectrophotometer. PL quantum efficiency data were measured on a Hamamatsu UV-NIR (C13534) absolute PL quantum yield spectrometer. Transient PL decay profiles at RT under N$_2$ atmosphere were recorded on a Horiba Jobin Yvon FluoroHub-B equipped with a single photon counting controller. Single crystal X-ray diffraction data was obtained on an Xcalibur E X-ray single crystal diffractometer equipped with a graphite monochromator Mo-Kα (λ = 0.71073 Å) radiation. Single crystal samples of **SAC-BOC** were obtained by slow evaporation of saturated solution from mixed solvents (dichloromethane and ethanol) at room temperature. The crystallographic data for **SAC-BOC** reported here has been deposited in the Cambridge Structural Database with CCDC number of 2308268.

Computational method. The initial geometry of **SAC-BOC** was extracted from its single crystal structure and then further optimized. The geometry of the ground state (S$_0$) was optimized at density functional theory (DFT) level using B3LYP hybrid functional and 6-31G(d) basis. The geometries of the excited states were optimized using time-dependent DFT (TD-DFT) method with CAM-B3LYP density functional. Furthermore, the energy of individual excited states was obtained using ωB97XD functional with a basis of 6-31+G(d)

based on their respective optimized molecular geometries accordingly. The calculations described above were performed using Gaussian 16 software package. The solvent effect in all the calculations was conducted using the polarizable continuum model (toluene). ORCA 5.0.4 program was used to obtain spin-orbit coupling matrix element (ζ) between lowest-lying singlet excited state and triplet excited states of **SAC-BOC**[1].To calculate the reorganization energy, the Dushin program was utilized.[2] The associated Huang-Rhys factor (S) was calculated with $S_i=\lambda_i/(h \cdot v_i)$ formula. Here, the symbol λ_i represents the decomposed reorganization energy, v_i denotes the frequency of normal vibration mode, h represents Planck constant.

2. Synthetic procedures and characterization data
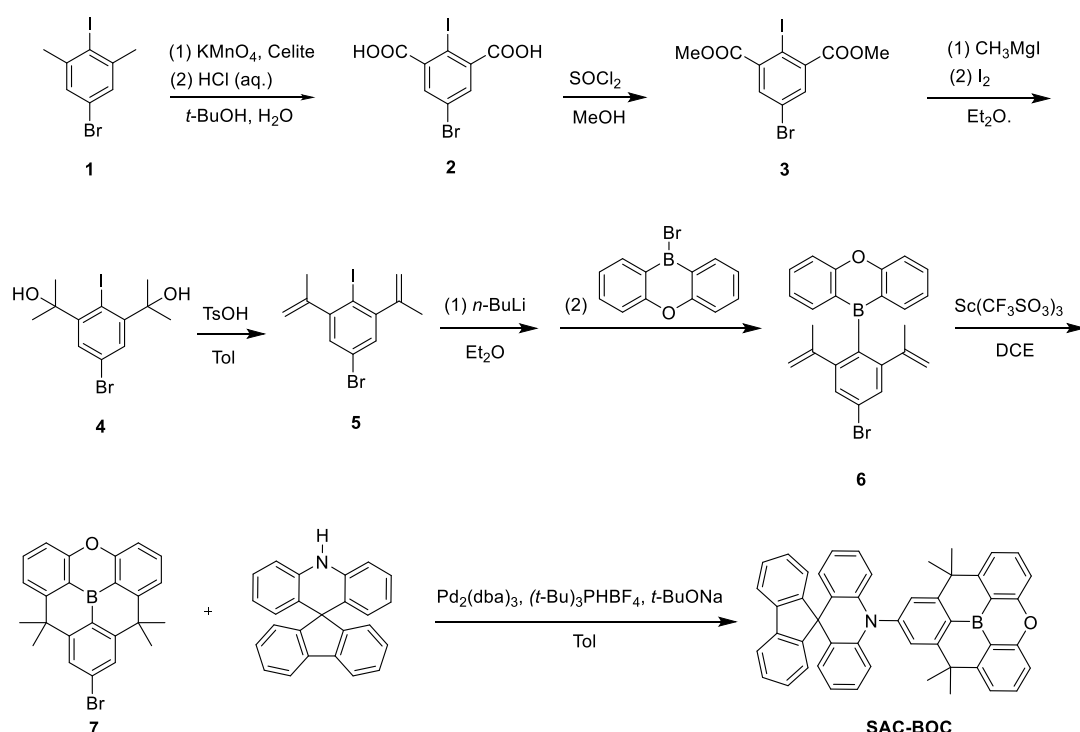
Scheme S1. Synthetic route to compound **SAC-BOC**.

The intermediates **2** and **3** were synthesized according to reported procedures.[3]

Synthesis of 1,1'-(5-bromo-2-iodo-1,3-phenylene)bis(ethan-1-ol) (4)

To a solution of **3** (12 g, 30 mmol) in toluene (100 mL), a Grignard reagent, CH$_3$MgI (60 mL, 3.0 M, 180 mmol), was slowly added. The reaction mixture was refluxed with continuous stirring for 2 hours. After that, I$_2$ (11.4 g, 45 mmol) in THF (50 mL) was slowly added. The reaction mixture was stirred at room temperature for 1 hour. The reaction was quenched by adding saturated aqueous solutions of NH$_4$Cl and Na$_2$S$_2$O$_3$. The organic layer was extracted with dichloromethane (DCM) three times. Subsequently, the organic extracts were washed

using a saturated aqueous solution of NaHCO₃ and brine, then dried over $MgSO_4$, filtration and evaporated under reduced pressure. The mixture was purified by recrystallization with DCM. This step yielded 5.45 g of **4** in a 45.5% yield as a faint yellow solid. ^{1}H NMR (400 MHz, CDCl₃) δ (ppm): 7.71 (s, 2H, ArH),1.84 (s, 12H, CH₃).

Synthesis of 5-bromo-2-iodo-1,3-di(prop-1-en-2-yl)benzene (5)

In a reaction vessel, a solution of **4** (2.77g, 6.94 mmol) and *p*-toluenesulfonic acid (0.239 g, 1.39 mmol) in toluene (35 mL) was heated under reflux in air for 1 hour. After cooling to room temperature, the reaction mixture was neutralized by addition of a saturated aqueous solution of NaHCO₃. Then the organic layer was extracted with DCM three times. The organic extracts were washed with brine and dried over $MgSO_4$. The solution was then filtered, and volatiles were evaporated under reduced pressure. The crude product was further purified using column chromatography on silica gel with PE (Petroleum ether) as the eluent. This step yielded 2.38 g of **5** in a 95% yield as a white solid. ^{1}H NMR (400 MHz, CDCl₃) δ (ppm): 7.18 (s, 2H, ArH), 5.22 (s, 2H, CH), 4.90 (s, 2H, CH), 2.06 (s, 6H, CH₃).

Synthesis of 10-(4-bromo-2,6-di(prop-1-en-2-yl)phenyl)-10*H*-dibenzo[*b*,*e*][1,4]oxaborinine (6)

At −78 °C, a solution of *n*-BuLi in hexane (6.25 mmol, 2.5 M, 2.5 mL,) was added dropwise to a solution of **5** (2 g, 5.53 mmol) in dry ether (80 mL). The resulting mixture was at this temperature for 1 hour. A solution of 9-bromo-9,10-dihydro-9-boraanthracene (Prepared from bis[2-(trimethylsilanyl)-phenyl] ether (1.6g, 6.18 mmol) and BBr₃ (7.0 mmol) according to the reference,[4] the difference is that the reaction solvent and remaining BBr₃ are directly removed by a vacuum oil pump equipped with cold hydrazine, and then the resulted yellow compound is dissolved in dry ether for the next reaction step) in dry (20 mL) was then added dropwise to the reaction mixture at −78 °C. After the addition was completed, the reaction mixture was allowed to slowly rise to room temperature and stirred overnight. The reaction was quenched with a saturated aqueous solution of NaHCO₃ and extracted with DCM three times. The organic extracts were washed with brine and dried over $MgSO_4$. After filtration, volatiles were evaporated under reduced pressure. The crude product was further purified by column chromatography on silica gel using PE as the eluent. This step gave 1.18g of **6** as a white solid with a yield of 51.4%. ^{1}H NMR (400 MHz, CDCl₃) δ (ppm): 7.69-7.64 (m, 4H, ArH), 7.50 (d, *J* = 8.4 Hz, 2H, ArH) 7.46 (s, 2H, ArH) 7.19 (t, *J* = 7.2 Hz, 2H, ArH) 4.64 (s, 2H, CH) 4.46 (s, 2H, CH) 1.87 (s, 6H, CH₃).

Synthesis of 10-bromo-8,8,12,12-tetramethyl-8,12-dihydro-4-oxa-3a²-boradibenzo[*cd,mn*]pyrene (7)

To a solution of **6** (1.0 g, 2.4 mmol) and Sc(OTf)$_3$ (2.36 g, 4.8 mmol) in 1,2-dichloroethane (800 mL), reflux was maintained with stirring for 4 days. The reaction mixture was allowed to cool to room temperature, following which a saturated aqueous solution of NaHCO$_3$ was added to it. The organic layer was extracted three times with dichloromethane, and the organic extract was dried over MgSO$_4$. After filtration, the volatiles were evaporated under reduced pressure. The crude product was purified using column chromatography on silica gel with PE as the eluent, giving 535 mg of **7** in 53.5% yield as a white solid. ^{1}H NMR (400 MHz, CDCl$_3$) δ (ppm): 7.81-7.77 (m, 4H, ArH), 7.51 (d, J = 7.6 Hz, 2H, ArH) 7.40 (d, J = 8.4 Hz, 2H, ArH) 1.78 (s, 12H, CH$_3$).

Synthesis of 10-(8,8,12,12-tetramethyl-8,12-dihydro-4-oxa-3a²-boradibenzo[*cd,mn*]pyren-10-yl)-10*H*-spiro[acridine-9,9'-fluorene] (SAC-BOC)

In a Schlenk tube, 235 mg (0.57 mmol) of **7**, 216 mg (0.65 mmol) 10*H*-spiro[acridine-9,9'-fluorene], 52 mg (0.057 mmol) of tris(dibenzylideneacetone)dipalladium, 66 mg (0.23 mmol) of tri-*tert*-butylphosphine tetrafluoroborate, 140 mg (1.5 mmol) of sodium *tert*-butoxide and 6 mL dry toluene were charged. Degassed by 3 cycles of freeze-pump-thaw. The solution was stirred at 110 °C for 48 hours. After cooling to room temperature, insoluble compounds were filtered under reduced pressure and the residue was washed with DCM. The solvent was evaporated and the crude compound was purified via column chromatography with PE: DCM = 5: 1 as solvent system and recrystallization, resulting in 250 mg of white powder product with a yield of 66%. ^{1}H NMR (400 MHz, CDCl3) δ(ppm): 7.84 (m, 4H, ArH), 7.73 (s, 2H, ArH), 7.58 (d, J = 7.6 Hz, 2H, ArH), 7.53 (t, J = 7.6 Hz, 2H, ArH), 7.46 (d, J = 8.0 Hz, 2H, ArH), 7.41 (t, J = 7.6 Hz, 2H, ArH), 7.32 (t, J = 7.6 Hz, 2H, ArH), 6.94 (m, 2H, ArH), 6.59 (t, J = 7.6 Hz, 2H, ArH), 6.45 (d, J = 8.0 Hz, 4H, ArH), 1.87 (s, 12H, CH$_3$). ^{13}C NMR (100 MHz, CDCl$_3$) δ 159.0, 158.9, 157.0, 155.8, 145.3, 141.4, 139.3, 134.7, 128.5, 128.0, 127.6, 127.4, 126.7, 126.0, 124.7, 120.5, 120.3, 119.9, 114.6, 113.7, 43.7, 34.1, 29.7. HRMS (ESI): calcd.: 666.2963 [M + H]$^+$; found: 666.2965.
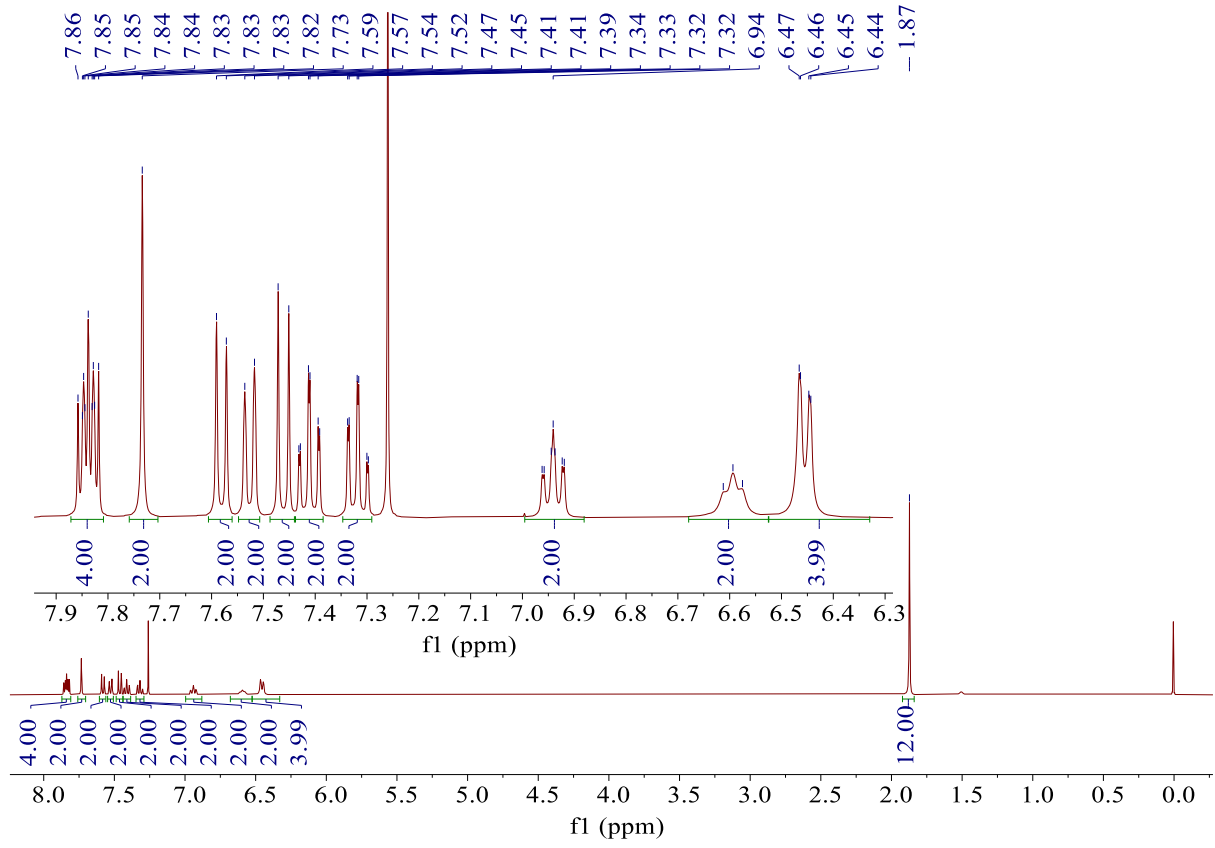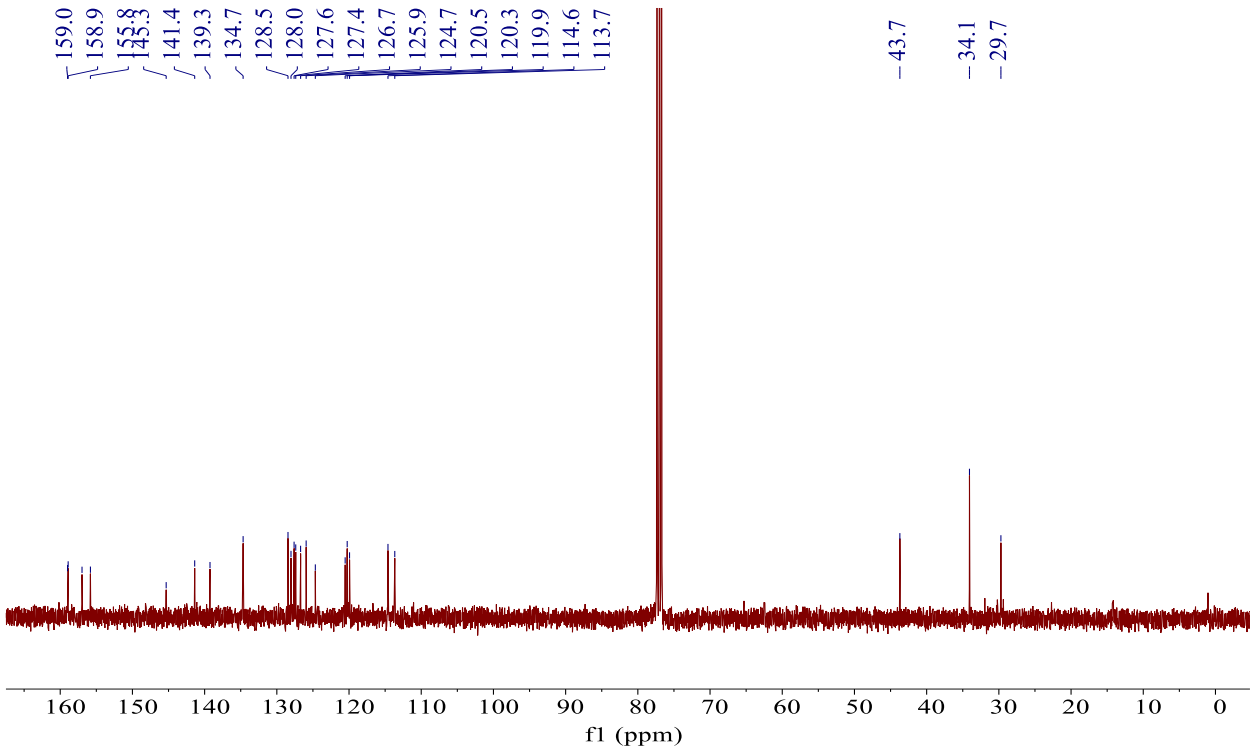
Fig. S1 The ^{1}H NMR spectrum of **SAC-BOC** in CDCl$_3$.

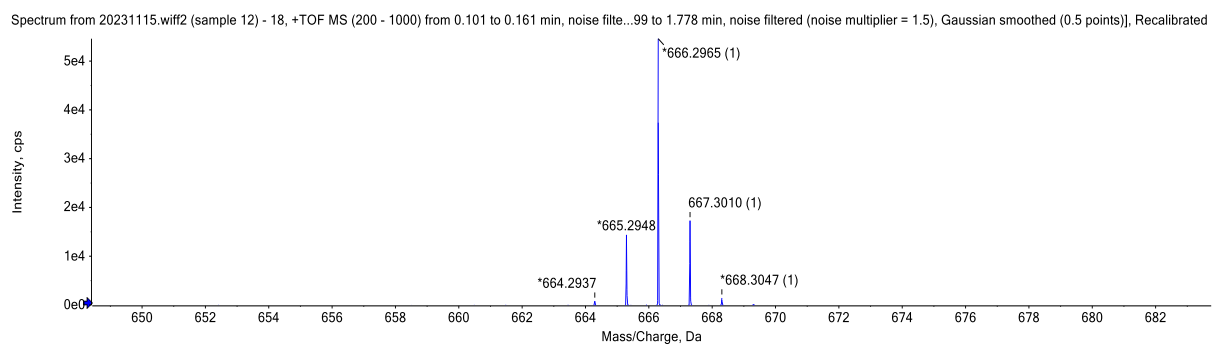**Fig. S2** The ^{13}C NMR spectrum of **SAC-BOC** in CDCl$_3$.

6

Fig. S3 The high resolution ESI mass spectrum of **SAC-BOC**. $C_{49}H_{36}BNOH^+$ $[M + H]^+$. Calcd.: 666.2963; found: 666.2965.
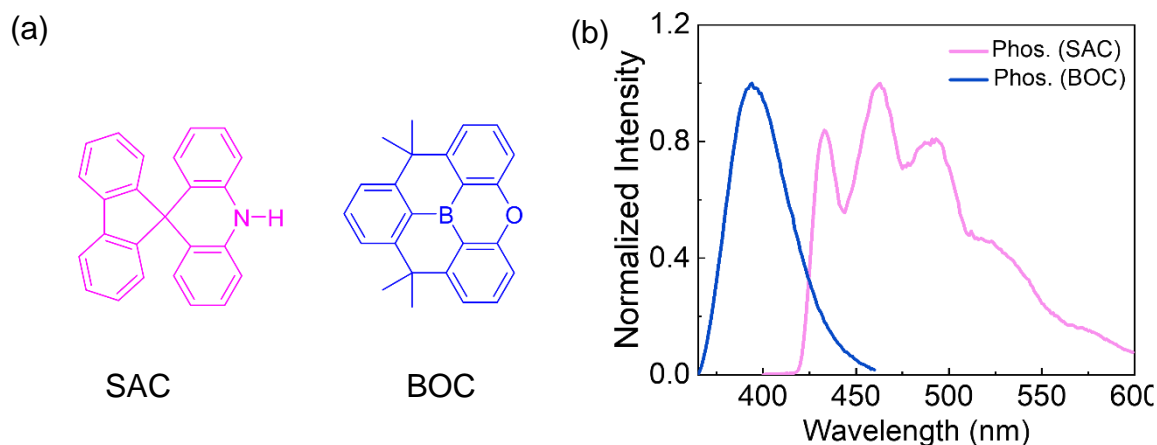
II. Characterization

Fig. S4 (a) The chemical structure of SAC and BOC. (b) Phosphorescence spectra of BOC in methyl cyclohexane (77 K, delay 200 ms) and SAC in 2-MeTHF (77 K, delay 10 ms).
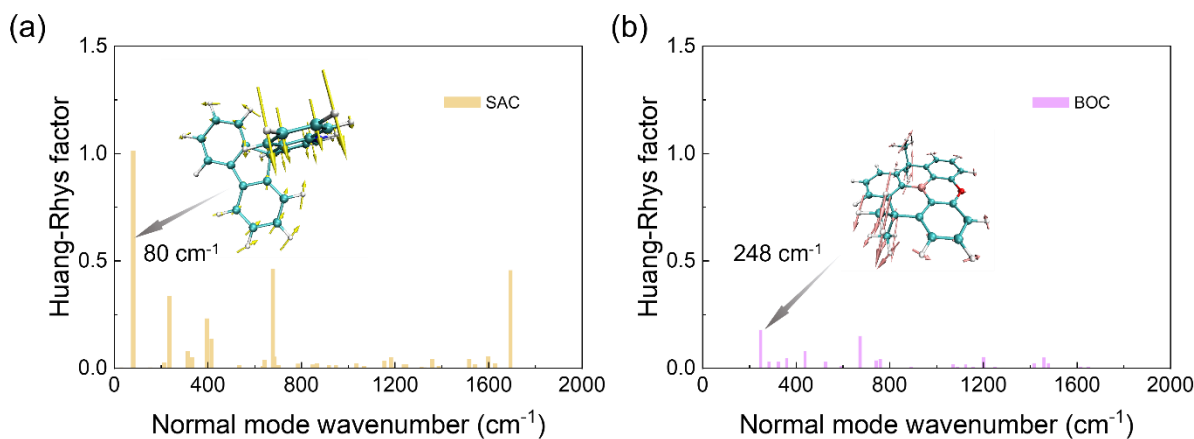

Fig. S5 (a) Huang-Rhys factor of a) SAC and b) BOC from the S_1 to S_0 states (inset: the vibration mode with the largest contribution to the Huang-Rhys factor).

The total reorganization energy (λ_{total}) between the S_0 and S_1 states was calculated to be 0.52 and 0.17 eV for SAC and BOC subunits, respectively. These relatively small λ_{total} for BOC and SAC units indicated the excellent structural rigidity for the both building units.

Table S1 Electrochemical, thermal stability properties and photophysical data.

E_{HOMO}[a] (eV)	E_{LUMO}[b] (eV)	T_m/T_d[c] (°C)	λ_{abs}[d] (nm)	λ_{em}[d] (nm)	FWHM[d] (nm)	ΔE_g[e] (eV)
−5.38	−2.38	352/381	356	455	61	3.00

[a] E_{HOMO} was calculated from the oxidation potential in dichloromethane. [b] E_{LUMO} was calculated according to the equation $E_{LUMO} = E_{HOMO} + \Delta E_g$. [c] Melting point /thermal decomposition temperature. [d] Measured in toluene (1×10^{-5} M). [e] Optical energy gap determined from absorption spectrum.

Table S2 Dynamics data of 20 wt% **SAC-BOC** doped film in DPEPO.

Φ_{PL}	Φ_{PF}	Φ_{DF}	τ_{PF} (ns)	τ_{DF} (μs)	k_{PF} $10^7 s^{-1}$	k_{DF} $10^5 s^{-1}$	k_r^s $10^7 s^{-1}$	k_{ISC} $10^7 s^{-1}$	k_{RISC} $10^5 s^{-1}$
63%	33%	30%	18	6.3	5.6	1.6	1.8	3.7	4.7

Φ_{PF} is the PLQY of prompt fluorescence component and Φ_{DF} is PLQY of TADF component; k_{PF} is prompt decay rate constant; k_{DF} is delayed decay rate constant; k_r^s is radiative rate constant of singlet excitons; k_{ISC} is intersystem crossing rate constant; k_{RISC} is reverse intersystem crossing rate constant.

$$\Phi_{PF} = \frac{k_r^s}{k_r^s + k_{nr}^s + k_{ISC}} \tag{1}$$

$$k_{PF} = \frac{1}{\tau_{PF}} \tag{2}$$

$$k_{DF} = \frac{1}{\tau_{DF}} \tag{3}$$

assuming, (i) $k_{PF} \gg k_{DF}$, (ii) $k_r^s \gg k_{nr}^s$, k_{RISC} and (iii) $k_{RISC} \gg k_r^T, k_{nr}^T$;

$$k_{PF} \approx k_r^s + k_{ISC} \tag{4}$$

$$k_{PF} \, k_{DF} \approx k_r^s \, k_{RISC} \tag{5}$$

$$k_{ISC} = k_{PF} \, \frac{\Phi_{DF}}{\Phi_{DF} + \Phi_{PF}} \tag{6}$$

$$\Phi_{PF} \approx \frac{k_r^s}{k_r^s + k_{ISC}} = \frac{k_r^s}{k_{PF}} \tag{7}$$

$$k_{ISC} \approx k_{PF} - k_r^s = k_{PF}(1 - \Phi_{PF}) \tag{8}$$

$$k_{RISC} \approx \frac{k_{PF} \cdot k_{DF}}{k_{PF} - k_{ISC}} \tag{9}$$

Table S3 Structure data of **SAC-BOC** single crystal.

Empirical formula	$C_{49}H_{36}BNO$ (2 CH_2Cl_2)
Formula weight	835.45
Temperature/K	150.0
Crystal system	triclinic
Space group	P-1
a/Å	9.2148(4)
b/Å	13.8751(7)
c/Å	16.7722(8)
α/°	74.990(2)
β/°	87.948(2)
γ/°	80.579(2)
Volume/Å^3	2043.28(17)
Z	2
ρcalcg/cm^3	1.358
μ/mm^{-1}	0.331
F(000)	868.0
Crystal size/mm^3	$0.44 \times 0.37 \times 0.1$
Radiation	MoKα (λ = 0.71073)
2Θ range for data collection/°	4.48 to 55.052
Index ranges	$-11 \le h \le 10$, $-18 \le k \le 18$, $-21 \le l \le 21$
Reflections collected	56158
Independent reflections	9376 [R_{int} = 0.1033, R_{sigma} = 0.0669]
Data/restraints/parameters	9376/0/527
Goodness-of-fit on F^2	1.038
Final R indexes [I>=2σ (I)]	R_1 = 0.0620, wR_2 = 0.1602
Final R indexes [all data]	R_1 = 0.0869, wR_2 = 0.1776
Largest diff. peak/hole / e Å^{-3}	0.80/-0.91
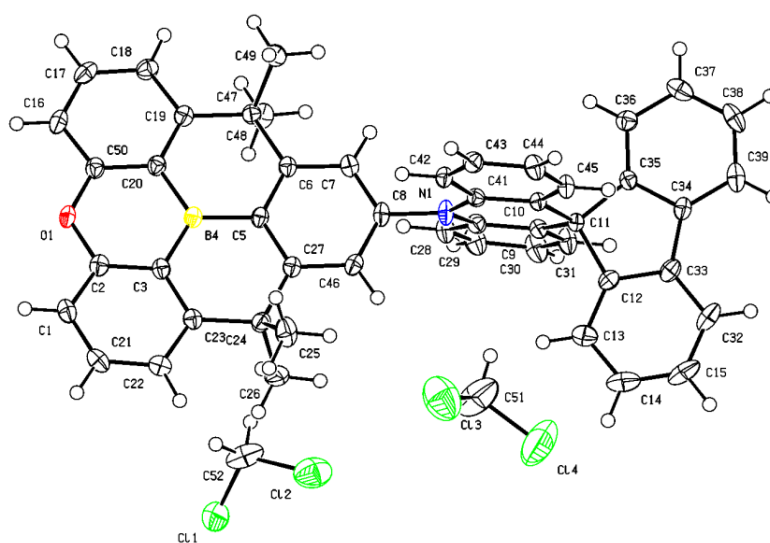
Fig. S6 ORTEP drawing of **SAC-BOC** with two dichloromethane solvent molecules (ellipsoids at 50% probability).

HOMO   LUMO
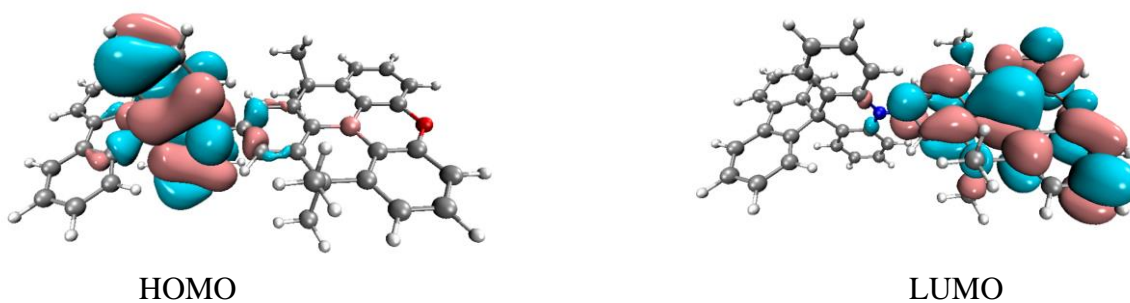
Fig. S7 The calculated HOMO and LUMO distributions of S_0 state.

Table S4 The natural transition orbitals (NTO) of **SAC-BOC** in different excited states revealed by TDDFT calculations by employing the ωB97xd functional with the 6-31+G(d) basis set.

Excited state	Hole	Particle	Eigenvalue	Transition nature
S_1			98.8%	CT
T_1			91.5%	CT-dominated
T_2			82.3%	LE_D
T_3			90.9%	LE_A-dominated

11
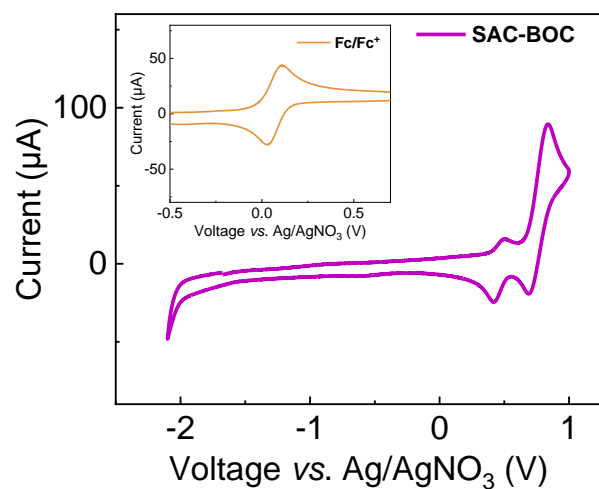
Fig. S8 Cyclic voltammogram of **SAC-BOC** measured at a scanning rate at 100 mV/s in 0.1 M solution of tetrabutylammonium hexafluorophosphate (TBAPF$_6$) in CH$_2$Cl$_2$. A Pt wire was used as the counter electrode and an Ag/Ag$^+$ electrode as the reference electrode.
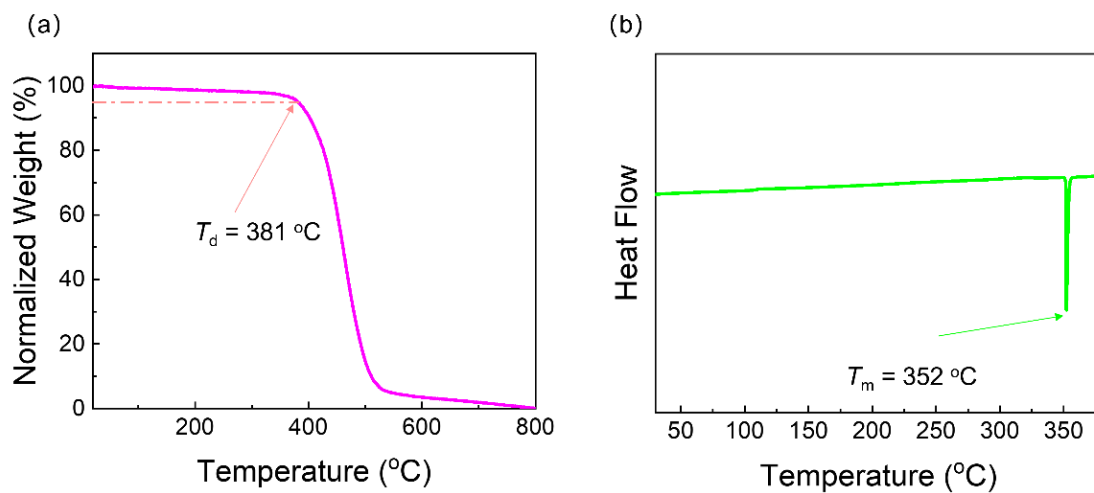
Fig. S9 (a)TGA and (b) DSC of **SAC-BOC**.
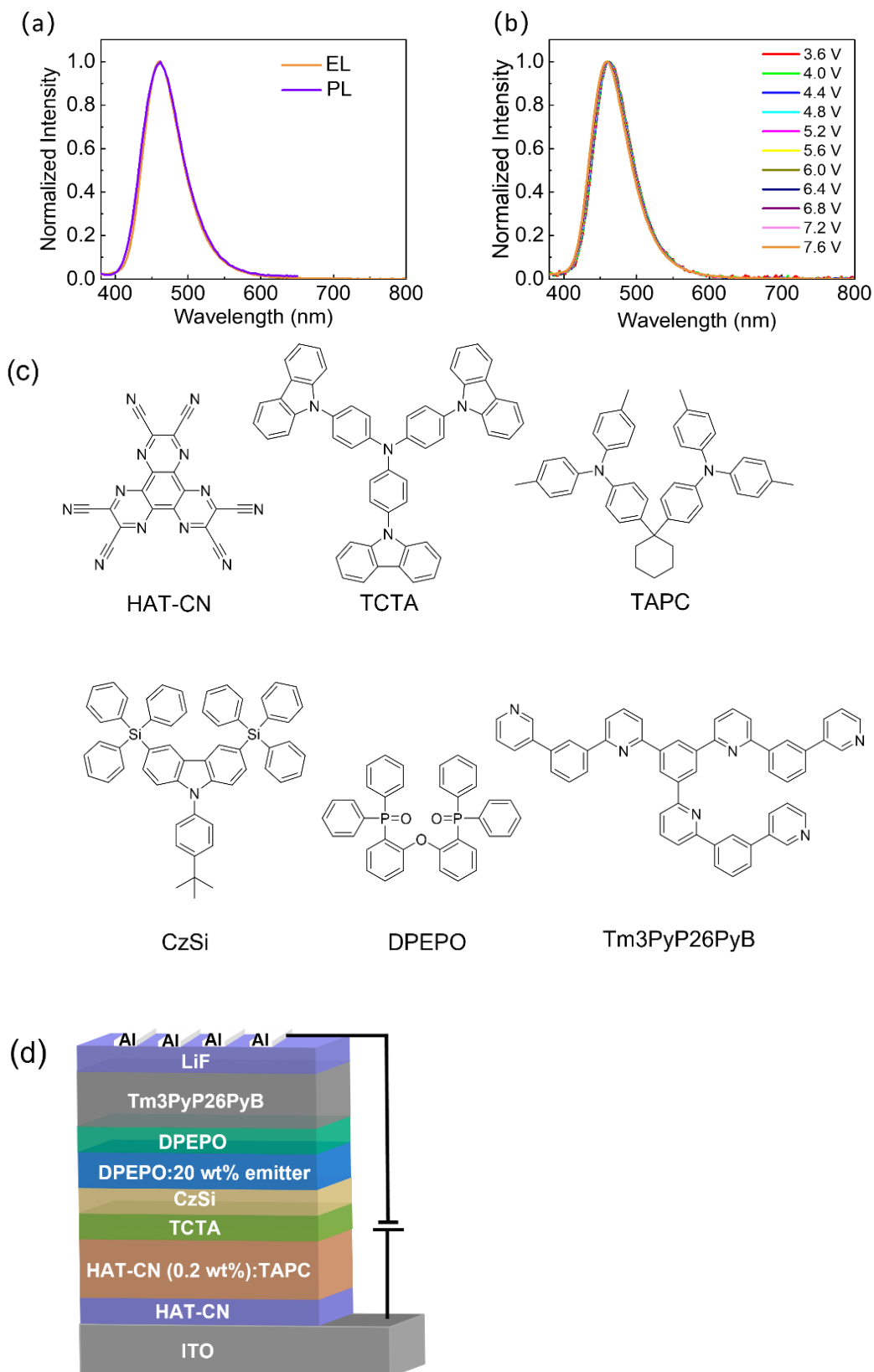
Fig. S10   (a) EL and PL spectra. (b) EL spectra under different driving voltages. (c) Chemical structures of the materials employed in the device. (d) Configuration of the OLED.

The light-emitting layer (EML) consists of the doped film with DPEPO as the host; ITO (indium tin oxide) and Al (aluminum) serve as the anode and cathode, respectively; HAT-CN (1,4,5,8,9,11-hexaazatriphenylene hexacarbonitrile) and LiF (lithium fluoride) are employed as the hole- and electron-injecting materials, respectively; the doping of 0.2 wt% HAT-CN into TAPC (1,1-bis(4-(N,N-di(p-tolyl)amino)phenyl)cyclo-hexane) can not only help to facilitate the hole injection process from the ITO anode into the TAPC organic layer, thus improve the balance of holes and electrons within the EML, but also help to reduce the device operation voltage; TCTA (tris(4-(9H-carbazol-9-yl)phenyl)amine), as well as Tm3PyP26PyB (1,3,5-tris(6-(3-(pyridin-3-yl)phenyl)pyridin-2-yl)benzene) act as the hole- and electron-transporting materials, respectively; CzSi (9-(4-tertbutylphenyl)-3,6-bis(triphenylsilyl)-9H-carbazole) and DPEPO are adopted as exciton-blocking materials to confine excitons within EML due to their high triplet energy levels.

Table S5 Summarized the **SAC-BOC**-based device data.

V_{on} (V)	$\lambda_{EL,max}$ (nm)	FWHM (nm)	L_{max} (cd·m^{-2})	CE_{max} (cd/A)	PE_{max} (lm/W)	EQE_{max}	$CIE_{x,y}$
3.5	460	57	112	16.1	14.4	15.3%	(0.144, 0.129)
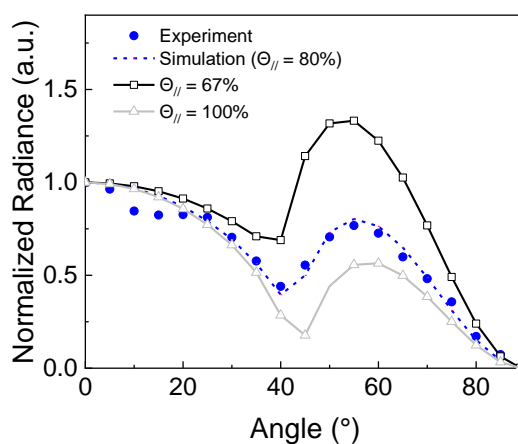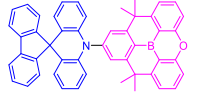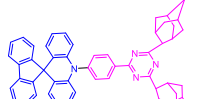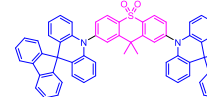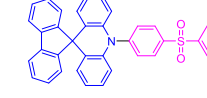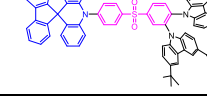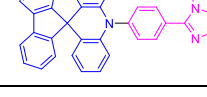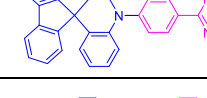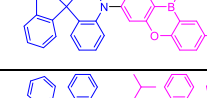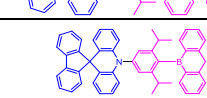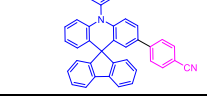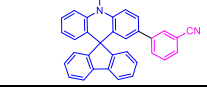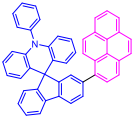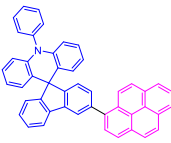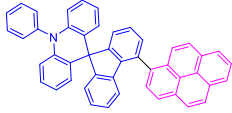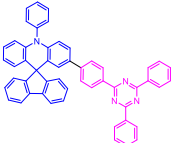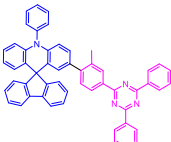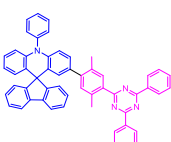
Figure S11. *p*-polarized angle-dependent PL radiance of the 20 wt% **SAC-BOC** doped film in DPEPO matrix.

III. Summary of the performance of reported purely organic small-molecule deep blue-OLEDs based on the SAC unit.

Table S6 Summary of the performance of deep-blue OLEDs based on the SAC unit reported so far.

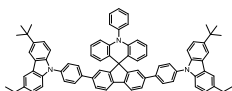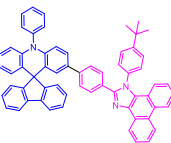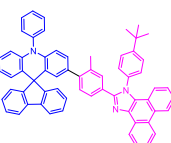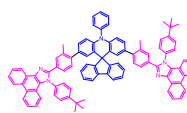| Name	Compound	$\lambda_{em,EL}$ (nm)	EQE_{max}	CE_{max} (cd/A)	PE_{max} (lm/W)	FWHM (nm)	CIE (x, y)	Ref.
SAC-BOC		460	15.3%	16.1	14.4	57	(0.144, 0.129)	This work
FA–TA		454	11.2%	-	-	69 [a]	(0.15, 0.13)	[5]
SPAC-DMT		455[a]	9.0%	11.4	-	42 [a]	(0.15, 0.13)	[6]
D1-DPS		441	4.13%	-	-	54 [a]	(0.153, 0.064)	[7]
3,4-Cz-SF-SFAC		457	31.05%	37.23	38.95	78 [a]	(0.15, 0.15)	[8]
imM-SPAC		451[a]	11.8%	14.0	13.0	70 [a]	(0.16, 0.15)	[9]
PM-SPAc		438	3.7%	3.01	1.39	83 [a]	(0.16, 0.12)	[10]
TDBA-SAF		456	28.2%	23.7	19.9	55 [a]	(0.142, 0.090)	[11]
sAC-sDBB		444	25.4%	14.8	13.7	49	(0.151, 0.058)	[12]
sAC-DBB		437	16.2%	8.7	6.8	50	(0.166, 0.066)	[12]
SAFpCN		432	4.63%	6.54	5.63	56	(0.153, 0.054)	[13]
SAFmCN		413	3.18%	3.86	2.50	50	(0.160, 0.046)	[13]

TFPy2		414	3.8%	1	0.84	51	(0.15, 0.03)	[14]
TFPy3		406	4.8%	0.5	0.43	50	(0.16, 0.02)	[14]
TFPy4		404	5.1%	0.5	0.40	54	(0.16, 0.02)	[14]
DTPSAF		460	5.7%	-	6.9	67	(0.143, 0.131)	[15]
DTTSAF		448	6.2%	-	4.8	68	(0.147, 0.096)	[15]
DTXSAF		444	7.7%	-	5.2	68	(0.149, 0.082)	[15]
SAF-2CzB		440	0.48%	4.07	1.83	-	(0.161, 0.111)	[16]
SAF-BPI		448	-	3.95	2.08	-	(0.15,0.10)	[17]
SAFPI		428	4.57%	2.90	2.84	55	(0.156, 0.053)	[18]
SAFDPI		432	4.77%	4.23	4.39	61	(0.154, 0.092)	[18]

[a] Estimated value according to the spectra in the literatures.

IV. References

1. F. Neese, *Wiley Interdiscip. Rev.: Comput. Mol. Sci.*, 2022, **12**, e1606.
2. J. R. Reimers, *J. Chem. Phys.*, 2001, **115**, 9103-9109.
3. A. Shuto, T. Kushida, T. Fukushima, H. Kaji and S. Yamaguchi, *Org. Lett.*, 2013, **15**, 6234-6237.
4. M. Melaïmi, S. Solé, C.-W. Chiu, H. Wang and F. P. Gabbaï, *Inorg. Chem.*, 2006, **45**, 8136-8143.
5. Y. Wada, S. Kubo and H. Kaji, *Adv. Mater.*, 2018, **30**, 1705641.
6. D. H. Ahn, J. H. Jeong, J. Song, J. Y. Lee and J. H. Kwon, *ACS Appl. Mater. Interfaces*, 2018, **10**, 10246-10253.
7. I. H. Lee, K. J. Kim, Y. K. Kim, Y. S. Kim and D. Myung, *J. Nanosci. Nanotechnol.*, 2019, **19**, 4583-4589.
8. J. Zhang, D. Li, W. Li, Y. Meng and Z. Ge, *Laser Photonics Rev.*, 2023, 2300758.
9. R.-H. Yi, G.-Y. Liu, Y.-T. Luo, W.-Y. Wang, H.-Y. Tsai, C.-H. Lin, H.-L. Shen, C.-H. Chang and C.-W. Lu, *Chem. Eur. J.*, 2021, **27**, 12998-13008.
10. B. Li, Z. Ding, Z. Wu, M. Liu, S. Chen, D. Chen, Z. Li, L. Sang, Y. Liu, L. Lin, W. Zhu and X. Wan, *Chem. Eng. J.*, 2023, **476**, 146484.
11. H. Lim, H. J. Cheon, S.-J. Woo, S.-K. Kwon, Y.-H. Kim and J.-J. Kim, *Adv. Mater.*, 2020, **32**, 2004083.
12. G. Xia, C. Qu, Y. Zhu, J. Ye, K. Ye, Z. Zhang and Y. Wang, *Angew. Chem., Int. Ed.*, 2021, **60**, 9598-9603.
13. T. Sudyoadsuk, S. Petdee, C. Kaiyasuan, C. Chaiwai, P. Wongkaew, S. Namuangruk, P. Chasing and V. Promarak, *J. Mater. Chem. C*, 2021, **9**, 6251-6256.
14. S.-N. Zou, X. Chen, S.-Y. Yang, S. Kumar, Y.-K. Qu, Y.-J. Yu, M.-K. Fung, Z.-Q. Jiang and L.-S. Liao, *Adv. Opt. Mater.*, 2020, **8**, 2001074.
15. S.-J. Woo, Y. Kim, M.-J. Kim, J. Y. Baek, S.-K. Kwon, Y.-H. Kim and J.-J. Kim, *Chem. Mater.*, 2018, **30**, 857-863.
16. W. Sun, N. Zhou, Y. Xiao, S. Wang and X. Li, *Dyes Pigm.*, 2018, **154**, 30-37.
17. W. Sun, N. Zhou, Y. Xiao, S. Wang and X. Li, *Chem. Asian J.*, 2017, **12**, 3069-3076.
18. C. Kaiyasuan, P. Chasing, P. Nalaoh, P. Wongkaew, T. Sudyoadsuk, K. Kongpatpanich and V. Promarak, *Chem. Asian J.*, 2021, **16**, 2328-2337.